# Covalent Template Approach Toward Functionalized Oligo-Alkyl-Substituted Shape-Persistent Macrocycles: Synthesis and Properties of Rings with a Loop

Andreas Ziegler,[†] Wael Mamdouh,[‡] An Ver Heyen,[‡] Mathieu Surin,[§] Hiroshi Uji-i,[‡] Mohammed M. S. Abdel-Mottaleb,[‡] Frans C. De Schryver,[‡] Steven De Feyter,*[,‡] Roberto Lazzaroni,*[,§] and Sigurd Höger*[,||]

*Max Planck Institute for Polymer Research, Ackermannweg 10, 55128 Mainz, Germany, Laboratory of Photochemistry and Spectroscopy, Division of Molecular and Nano Materials, Department of Chemistry, Katholieke Universiteit Leuven (K. U. Leuven), Celestijnenlaan 200 F, 3001 Leuven, Belgium, Service de Chimie des Matériaux Nouveaux, Université de Mons-Hainaut, Place du Parc 20, 7000 Mons, Belgium, and Institut für Technische Chemie und Polymerchemie, Universität Karlsruhe (TH), Engesserstr. 18, 76131 Karlsruhe, Germany*

*Received June 27, 2005. Revised Manuscript Received September 5, 2005*

The synthesis, properties, and conformation of shape-persistent macrocycles with extraannular oligo-alkyl groups and an intraannular bis(hydroxymethyl)biphenylene diester are investigated. The key step in the preparation is the template-supported Glaser coupling of rigid bisacetylenes which allows obtaining the cyclic product in 81% yield. Contrary to the initial expectations, the compounds do not exhibit liquid crystalline phases. This could be explained by a nonplanar conformation of the molecules because the biphenylene bridge is longer than the diameter of the rings. On the other hand, scanning tunneling microscopy investigations indicate that the intraannular biphenylene bridge can be located in the same plane as the aromatic backbone of the macrocycles on graphite. Modeling involving molecular mechanics and molecular dynamics simulations unraveled this apparent inconsistency by showing that the molecules adopt a nonplanar conformation in the absence of the solid support whereas planarization takes place when they are adsorbed on the graphite surface.

## Introduction

Shape-persistent macrocycles based on the phenylene, phenylene−ethynylene, and phenylene−butadiynylene backbone have attracted increasing interest during the last years.[1] They are composed of a rigid molecular backbone and flexible (functional) side groups that ensure their processability. The side group orientation together with their polarity determines the properties and applications of the macrocycles. For example, macrocycles with polar functionalities orthogonal to the molecular backbone can form one-dimensional superstructures. Rings with extraannular polar groups can form two-dimensional layer structures, and compounds with intraannular polar groups are able to recognize appropriate guest molecules.[2−4] During the last years we have focused on the synthesis and the one- and two-dimensional organization of shape-persistent phenylene−ethynylene macrocycles by using nonspecific interactions. For example, solvophobic interactions enabled us to induce the aggregation of coil−ring−coil block structures to form supramolecular hollow polymer brushes.[1f,5] Oligo-alkyl-substituted macrocycles, like **1** (Chart 1), could be organized

* To whom correspondence should be addressed. Dr. S. De Feyter: fax (+32)-16-327-990, e-mail Steven.DeFeyter@chem.kuleuven.be. Prof. Dr. R. Lazzaroni: fax (+32)65-373-861, e-mail roberto@averell.umh.ac.be. Prof. Dr. S. Höger: fax (+49)721-608-3151, e-mail hoeger@chemie.uni-karlsruhe.de.

[†] Max Planck Institute for Polymer Research.

[‡] Katholieke Universiteit Leuven.

[§] Université de Mons-Hainaut.

[||] Universität Karlsruhe.

(1) For recent reviews on shape-persistent macrocycles see, for example: (a) Moore, J. S. *Acc. Chem. Res.* **1997**, *30*, 402−413. (b) Höger, S. *J. Polym. Sci., Part A: Polym. Chem.* **1999**, *37*, 2685−2698. (c) Haley, M. M.; Pak, J. J.; Brand, S. C. *Top. Curr. Chem.* **1999**, *201*, 81−130. (d) Grave, C.; Schlüter, A. D. *Eur. J. Org. Chem.* **2002**, 3075−3098. (e) Zhao, D.; Moore, J. S. *Chem. Commun.* **2003**, 807−818. (f) Höger, S. *Chem.—Eur. J.* **2004**, *10*, 1320−1329. (g) *Acetylene Chemistry*; Diederich, F., Stang, P. J., Tykwinski, R., Eds.; Wiley-VCH: Weinheim, 2005.

(2) For adaptable side groups see, for example: (a) Höger, S.; Enkelmann, V. *Angew. Chem.* **1995**, *107*, 2917−2919; *Angew. Chem., Int. Ed. Engl.* **1995**, *34*, 2713−2716. (b) Morrison, D. L.; Höger, S. *J. Chem. Soc., Chem. Commun.* **1996**, 2313−2314. (c) Höger, S.; Morrison, D. L.; Enkelmann, V. *J. Am. Chem. Soc.* **2002**, *124*, 6734−6736.

(3) For the aggregation of large macrocycles that may ultimately lead to one-dimensional channel structures see, for example: (a) Zhang, J.; Moore, J. S. *J. Am. Chem. Soc.* **1992**, *114*, 9701−9702. (b) Shetty, A. S.; Zhang, J.; Moore, J. S. *J. Am. Chem. Soc.* **1996**, *118*, 1019−1027. (c) Tobe, Y.; Nagano, A.; Kawabata, K.; Sonoda, M.; Naemura, K. *Org. Lett.* **2000**, *2*, 3265−3268. (d) Nakamura, K.; Okubo, H.; Yamaguchi, M. *Org. Lett.* **2001**, *3*, 1097−1099. (e) Tobe, Y.; Utsumi, N.; Kawabata, K.; Nagano, A.; Adachi, K.; Araki, S.; Sonoda, M.; Hirose, K.; Nakamura, K. *J. Am. Chem. Soc.* **2002**, *124*, 5350−5364. (f) Zhao, D.; Moore, J. S. *J. Org. Chem.* **2002**, *67*, 3548−3554. (g) Saiki, Y.; Sugiura, H.; Nakamura, K.; Yamaguchi, M.; Hoshi, T.; Anzai, J. *J. Am. Chem. Soc.* **2003**, *125*, 9268−9269. (h) Gallant, A. J.; MacLachlan, M. J. *Angew. Chem.* **2003**, *115*, 5465−5468; *Angew. Chem., Int. Ed.* **2003**, 42, 5307−5310. (i) Ryu, J.-H.; Oh, N.-K.; Lee, M. *Chem. Commun.* **2005**, 1770−1772.

(4) For two-dimensional superstructures based on shape-persistent macrocycles see, for example: (a) Venkataramen, D.; Lee, S.; Zhang, J.; Moore, J. S. *Nature* **1994**, *371*, 591−593. (b) Krömer, J.; Rios Carreras, I.; Fuhrmann, G.; Musch, C.; Wunderlin, M.; Debaerdemaeker, T.; Mena-Osteritz, E.; Bäuerle, P. *Angew. Chem.* **2000**, *112*, 3623−3628; *Angew. Chem., Int. Ed.* **2000**, *39*, 3418−3486. (c) Grave, C.; Lentz, D.; Schäfer, A.; Samori, P.; Rabe, J. P.; Franke, P.; Schlüter, A. D. *J. Am. Chem. Soc.* **2003**, *125*, 6907−6918. (d) Kalsani, V.; Ammon, H.; Jäckel, F.; Rabe, J. P.; Schmittel, M. *Chem.—Eur. J.* **2004**, *10*, 5481.

10.1021/cm051386l CCC: $30.25 
Published on Web 10/19/2005

**Chart 1**

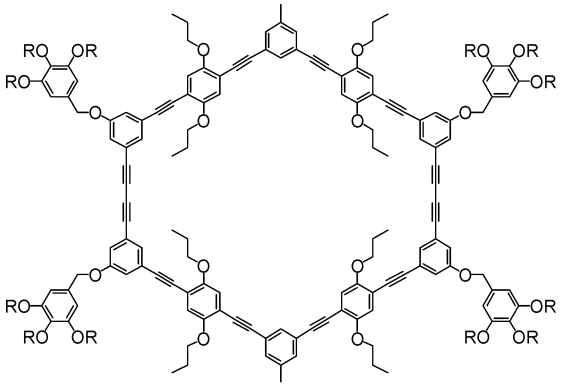

**1**: R = $C_{12}H_{25}$

**Chart 2**

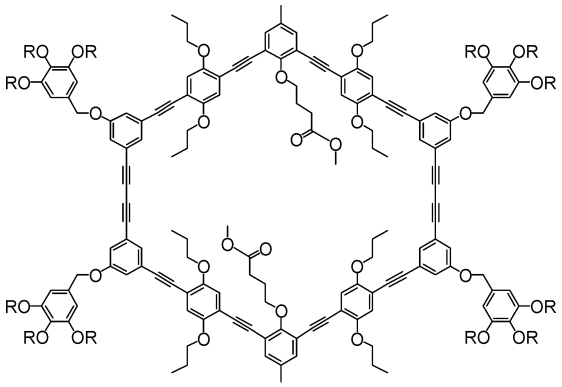

**2a**: R = $C_{12}H_{25}$
**2b**: R = $C_{16}H_{33}$

in two dimensions when physisorbed from solution onto the surface of an appropriate solid substrate leading to regular surface patterns on the nanometer scale.[6] Specifically, **1** forms an extended two-dimensional lattice on the surface of highly oriented pyrolytic graphite (HOPG). The driving force for the adsorption of the macrocycles at the surface is the nonspecific attractive van der Waals interaction of the rigid and the flexible ring parts, including the alkyl chains, with the graphite surface. Under the assumption that the superstructure formation is only sparingly affected by a manipulation of the ring interior, these macrocycles may lead to functionalized superstructures after the addition of appropriate functional groups.

Subsequent investigations on appropriate macrocycles that contain additional intraannular polar groups (**2**, Chart 2) show that these compounds also adsorb at the surface of graphite exhibiting similar lattice parameters. However, the additional ester functionality in **2** somewhat affects the pattern formation. When physisorbed from 1-phenyloctane, the macrocycles are locally ordered to a certain degree but do not form a two-dimensional crystal.[7] This can be explained by taking into account that the ability of the molecules to form a two-dimensional crystal is strongly influenced by the adsorption/desorption equilibrium and the delicate balance between molecule−molecule and molecule−substrate interactions. Accordingly, the solvent from which the macrocycles were adsorbed also influences the pattern formation, and **2**, physisorbed from 1,2,4-trichlorobenzene (TCB), forms more ordered arrays, although the resolution of the scanning tunneling microscopy (STM) images is worse. All these observations indicate that derivatives of **2**, and even other esters, should behave differently. Therefore, their investigation is desirable because it should provide further information on the molecular requirements for these compounds to form extended two-dimensional crystals on the graphite surface.

In a different work it has been shown that the ester groups of **2** allow further modifications of the ring interior and, therefore, the introduction of binding sites for other substrates. For example, functionalization of the interior of **2** with thioether groups leads to compounds that form ordered arrays on Au(111) substrates.[8,9] Crucial for all transformations of the ester groups in **2** and subsequent investigations is that the material is available in sufficient quantities. The previously reported synthesis of the macrocyclic backbone of **2** is based on the oxidative intermolecular Glaser coupling of the corresponding bisacetylenic precursors ("half-rings") under pseudo high-dilution conditions.[7] Although the diester **2** was prepared by this procedure on a 100-mg scale, the synthesis suffers from the fact that the intermolecular cyclization step gives the macrocycle in only 29% isolated yield as a result of its tedious purification by repeated column chromatography.[10] Because the half-rings are available only by a multistep synthesis, the investigation of alternative cyclization conditions is an attractive research goal. In recent studies we could show that functionalized shape-persistent macrocycles containing butadiyne units can be obtained in high yields if the acetylenic ring precursors are bound covalently to an appropriate template prior to the oxidative coupling.[11] The intraannular binding sites of **2** are ideal geometric prerequisites for the application of our *covalent template approach* and should give the macrocycles not only in much higher yield but should also lead to a much easier product purification.

Apart from the adsorption behavior of derivatives of **2**, the investigation of the thermal behavior of these compounds, especially the formation of mesophases, is of great interest. Thermotropic liquid crystals based on discotic mesogenes are valuable materials for a variety of different optical and

(5) (a) Rosselli, S.; Ramminger, A.-D.; Wagner, T.; Silier, B.; Wiegand, S.; Häussler, W.; Lieser, G.; Scheumann, V.; Höger, S. *Angew. Chem.* **2001**, *113*, 3234−3237; *Angew. Chem., Int. Ed.* **2001**, *40*, 3138−3141. (b) Höger, S.; Bonrad, K.; Rosselli, S.; Ramminger, A.-D.; Wagner, T.; Silier, B.; Wiegand, S.; Häussler, W.; Lieser, G.; Scheumann, V. *Macromol. Symp.* **2002**, *177*, 185−191. (c) Rosselli, S.; Ramminger, A.-D.; Wagner, T.; Lieser, G.; Höger, S. *Chem.—Eur. J.* **2003**, *9*, 3481−3491.

(6) Höger, S.; Bonrad, K.; Mourran, A.; Beginn, U.; Möller, M. *J. Am. Chem. Soc.* **2001**, *123*, 5651−5659.

(7) Fischer, M.; Lieser, G.; Rapp, A.; Schnell, I.; Mamdouh, W.; De Feyter, S.; De Schryver, F. C.; Höger, S. *J. Am. Chem. Soc.* **2004**, *126*, 214−222.

(8) Borissov, D.; Ziegler, A.; Höger, S.; Freyland, W. *Langmuir* **2004**, *20*, 2781−2784.

(9) **1** and **2** do not form a two-dimensional lattice on Au(111).

(10) According to the GPC data, the crude product of the cyclization contains 60−65% shape-persistent macrocyclic dimer.

(11) (a) Höger, S.; Meckenstock, A.-D.; Pellen, H. *J. Org. Chem.* **1997**, *62*, 4556−4557. (b) Höger, S.; Mechenstock, A.-D. *Tetrahedron Lett.* **1999**, *39*, 1735−1736. (c) Höger, S.; Meckenstock, A.-D. *Chem.—Eur. J.* **1999**, *5*, 1686−1691. (d) Höger, S. *Macromol. Symp.* **1999**, *142*, 185−191. (e) Fischer, M.; Höger, S. *Eur. J. Org. Chem.* **2003**, 441−446.

electrooptical applications.[12] This holds for discotics in the columnar phase, which have been used for photovoltaic applications, as well as discotics in the nematic phase, which are commercialized as compensation layers in display technology.[13,14] Discotic liquid crystals based on shape-persistent macrocycles are additionally interesting candidates for the formation of tubelike superstructures.[15] However, the structural requirements for the observation of liquid crystallinity in compounds based on the phenylene−ethynylene backbone, such as **1** or **2**, are not well-understood. Previous studies in our group indicated that intraannular substituents have a dramatic effect on the thermal behavior of these compounds. Shape-persistent macrocycles with extraannular linear C18 substituents melt isotropically while isomeric structures in which the alkyl groups point to the inside exhibit nematic phases.[16] This first hint that the large open cavity in the macrocycles counteracts the mesophase formation is supported by the fact that **1** does not exhibit liquid crystallinity while **2** forms a columnar mesophase over a broad temperature range. Accordingly, the investigation of the thermal behavior of other derivatives of **2** that are sufficiently substituted to fill their intraannular cavity should increase our insight into the structural parameters that are necessary to observe thermotropic mesophases in these macrocycles.

## Results and Discussion

**Synthesis.** Target structures of our synthesis are the macrocycles **16a** and **16b**. They can be viewed as biphenylene-bridged analogues of our previously described compounds **2a** and **2b**. The synthesis of the macrocycles is shown in Scheme 1.

Alkylation of 2,6-diiodo-4-methylphenol (**3**) with 4-bromotrimethylothobutyrate gave the ester **4** in 73% yield. Palladium-catalyzed Sonogashira−Hagihara coupling of **4** and **5** gave **6** (87%), and subsequent desilylation yielded the bisacetylene **7** (74%).[7] Base-promoted hydrolysis of **7** yielded the free acid **8** (72%), which was esterified with 4,4′-bis-(hydroxymethyl)biphenyl using diisopropylcarbodiimide (DIC) to give **9** (99%). The attachment of the four corner pieces that contain in the final structure the oligo-alkyl side groups can in principle be performed in several ways. Recent studies in our group have shown that bisacetylenes (not template-bound) can be treated with a 7−10-fold excess of an aromatic diiodide under the conditions of the Sonogashira−Hagihara coupling and give the corresponding (enlarged) diiodides in yields up to 80%.[7] However, here a 4-fold coupling of **9** with a large excess of the protected diiodophenol would have to be performed to obtain a template-bound tetraiodide (which could be subsequently transformed into the bisacetylenic ring precursors). After the first coupling of **9** with an aromatic diiodide, the subsequent three intermolecular coupling reactions (with the excess of diiodide) would have to compete with intramolecular coupling reactions and most probably lead to a complex reaction mixture.[17] The use of excess reagent was, therefore, avoided by coupling **9** with the monoiodide **10** to yield the silyl-protected tetraacetylene **11** (48%). The rather low isolated yield in this step was not expected. We ascribe this to side products arising from the oxidative acetylene dimerization (a common side reaction of the Sonogashira−Hagihara coupling) that could only be removed by repeated column chromatography. This shows the limits of the covalent template approach: to obtain the template-bound acetylenes in high yield the (quadruple) Sonogashira−Hagihara coupling reactions have to be performed with template-bound aryl iodides and excess (low-molecular-weight) acetylenes and not vice versa.[18,19] Monoiodide **10** was obtained by a statistical reaction of the corresponding THP-protected 3,5-diiodophenol and 3-cyanopropyldimethylsilylacetylene (CPDMS acetylene).[20] The CPDMS protecting group has a rather high polarity. In statistical reactions this makes the separation of the double-coupled side product and the remaining starting material relatively easy, even with large material quantities. Removal of the CPDMS group can be obtained under mild conditions, and treating **11** with tetrabutylammonium fluoride in tetrahydrofuran (THF) gave the templated bisacetylene **12** (76%). The cyclization of **12** under pseudo high-dilution conditions gave the template-bound macrocycle **13** in high yields, as detected by gel permeation chromatography (GPC), and **13** could be isolated in 81% yield. In addition to the higher product yield compared to the statistical intermolecular dimerization of the appropriate bisacetylenes, the covalent template approach has the advantage that the product is much easier purified. Acid-catalyzed deprotection of the THP groups gave the tetraphenol **14** in nearly quantitative yield. Base-catalyzed alkylation of **14** with **15a** and **15b** gave the template-bound oligo-alkyl-substituted macrocycles **16a** (59%) and **16b** (72%), respectively.

**16a** and **16b** were characterized by NMR spectroscopy, GPC, and matrix-assisted laser desorption ionization time-

(12) (a) Chandrasekhar, S.; Sadashiva, B. K.; Suresh, K. A. *Pramana* **1977**, *9*, 471−480. (b) Chandrasekhar, S. In *Handbook of Liquid Crystals*; Demus, D., Goodby, J., Gray, G. W., Spiess, H.-W., Vill, V., Eds.; Wiley-VCH: Weinheim, 1998; Vol. 2B, pp 749−780. (c) Bushby, R. J.; Lozman, O. R. *Curr. Opin. Colloid Interface Sci*. **2002**, *7*, 343−354.

(13) (a) Adam, D.; Schuhmacher, P.; Simmerer, J.; Haeussling, L.; Siemensmeyer, K.; Etzbach, K. H.; Ringsdorf, H.; Haarer, D. *Nature* **1994**, *371*, 141−143. (b) Boden, N.; Bushby, R. J.; Clements, J.; Movaghar, B. *J. Mater. Chem.* **1999**, *9*, 2081−2086. (c) Schmidt-Mende, L.; Fechtenkötter, A.; Müllen, K.; Moons, E.; Friend, R. H.; MacKenzie, J. D. *Science* **2001**, *293*, 1119−1122.

(14) (a) Mori, H.; Itoh, Y.; Nishiura, Y.; Nakamura, T.; Shinagawa, Y. *Jpn. J. Appl. Phys. A* **1997**, *36*, 143−147. (b) Okazaki, M.; Kawata, K.; Nishikawa, H.; Negoro, M. *Polym. Adv. Technol.* **2000**, *11*, 398−403. (c) Kumar, S.; Varshney, S. K. *Angew. Chem.* **2000**, *112*, 3270−3272; *Angew. Chem., Int. Ed*. **2000**, *39*, 3140−3142.

(15) (a) Behr, J. P.; Lehn, J.-M.; Dock, A.-C.; Moras, D. *Nature* **1982**, *295*, 526−527. (b) Lehn, J.-M.; Malthete, J.; Levelut, A.-M. *J. Chem. Soc. Chem. Commun.* **1985**, 1794−1796. (c) Zhang, J.; Moore, J. S. *J. Am. Chem. Soc.* **1994**, *116*, 2655−2656. (d) Mindyuk, O. Y.; Stetzer, M. R.; Heiney, P. A.; Nelson, J. C.; Moore, J. S. *Adv. Mater*. **1998**, *10*, 1363−1366.

(16) (a) Höger, S.; Enkelmann, V.; Bonrad, K.; Tschierske, C. *Angew. Chem.* **2000**, *112*, 2356−2358; *Angew. Chem., Int. Ed.* **2000**, *39*, 2268−2270. (b) Höger, S.; Cheng, X. H.; Ramminger, A.-D.; Rapp, A.; Mondeshki, M.; Schnell, I.; Enkelmann, V. *Angew. Chem*. **2005**, *117*, 2862−2866; *Angew. Chem., Int. Ed.* **2005**, *44*, 2801−2805.

(17) Because of its rigidity this is not the fact for the reaction of **7** with an excess of aromatic diiodides.

(18) It has been shown previously that in those cases the side products from the oxidative acetylene coupling could be easily removed.

(19) Alternatively, the ring precursors can be connected to the template at a later stage of the reaction sequence.

(20) Höger, S.; Bonrad, K. *J. Org. Chem.* **2000**, *65*, 2243−2245.

**Scheme 1**[a]

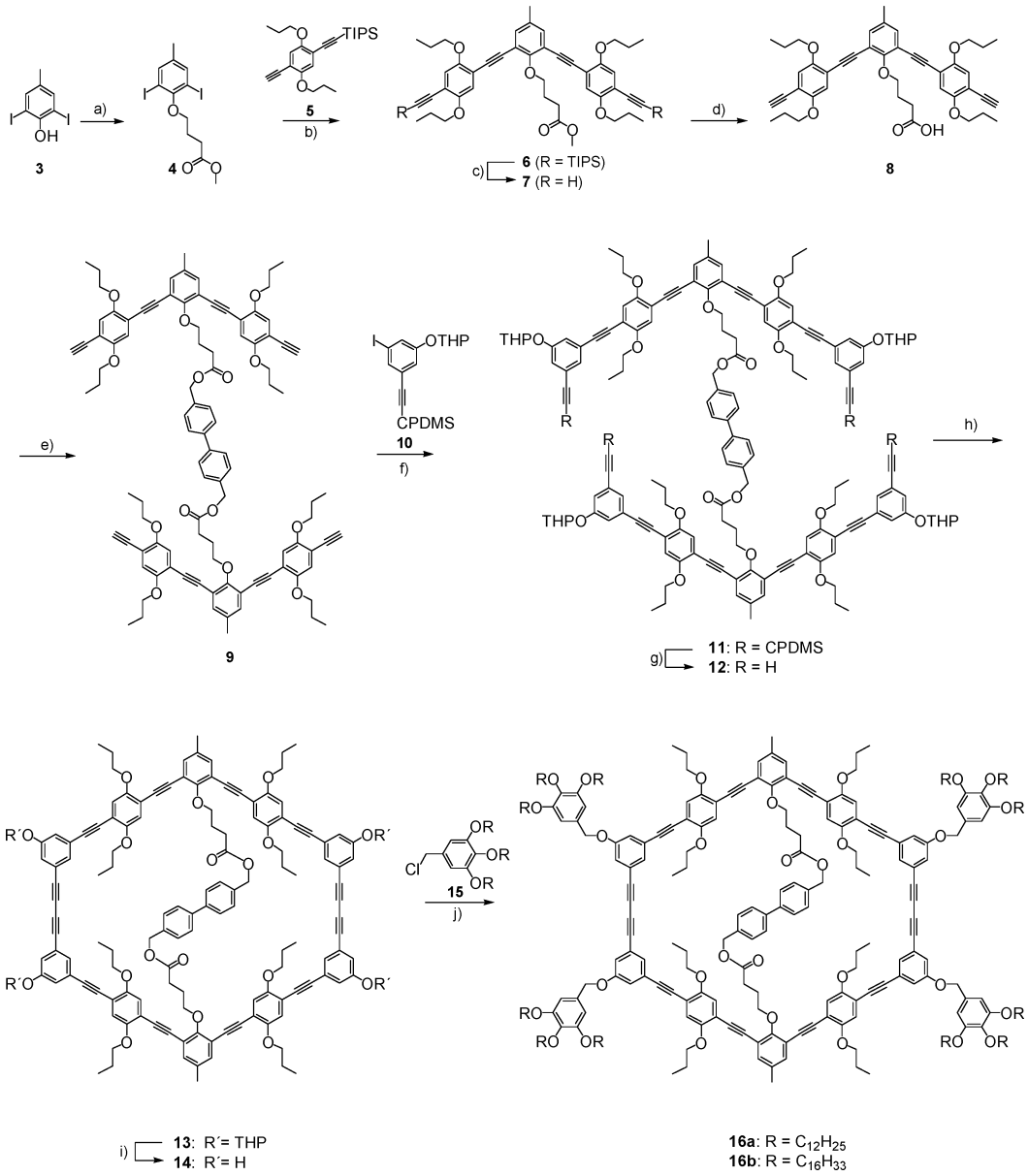


[a] (a) 4-Bromotrimethylorthobutyrate, $K_2CO_3$, DMF (73%); (b) $PdCl_2(PPh_3)_2$, CuI, $NEt_3$ (87%); (c) $Bu_4NF$, THF/$H_2O$ (74%); (d) $Bu_4NOH$, $H_2O$, THF (72%); (e) 4,4′-bis(hydroxymethyl)biphenyl, DIC (99%); (f) $PdCl_2(PPh_3)_2$, CuI, $NEt_3$/THF (48%); (g) $Bu_4NF$, THF (76%); (h) CuCl, $CuCl_2$, pyridine (81%); (i) *p*-TsOH, MeOH, $CHCl_3$ (99%); (j) $K_2CO_3$, DMF (59%, 72%).

of-flight (MALDI TOF) spectroscopy. In solution, the NMR spectra of **16a** and **16b** are alike and differ only in the integral of the methylene signals for the alkyl chains. The NMR spectra indicate full alkylation and show molecules with a high degree of symmetry. This indicates that the molecular dynamics (MD) in solution is not restricted by the template (Figure 1).

**Phase Behavior.** As already pointed out before, **1** does not exhibit a liquid crystalline phase while **2a** and **2b** show a discotic columnar liquid crystalline phase over a broad temperature range. The absence of a thermotropic mesophase in **1** can be explained by the assumption that the large internal void in the macrocycle leads to a conflict between the molecular anisotropy and the empty space inside the rings: because the filling of the cavity of **1** by a backfolding of the extraannular oligo-alkyl groups is rather improbable, the alkyl groups of adjacent rings have to fill that cavity. The competition between orientational correlation of the rigid parts of the macrocycles and the necessity of the alkyl chains

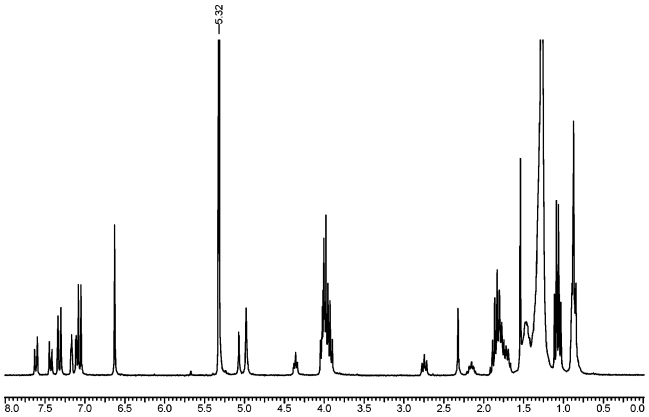


**Figure 1.** $^1H$ NMR spectrum of **16a** (in $CD_2Cl_2$).

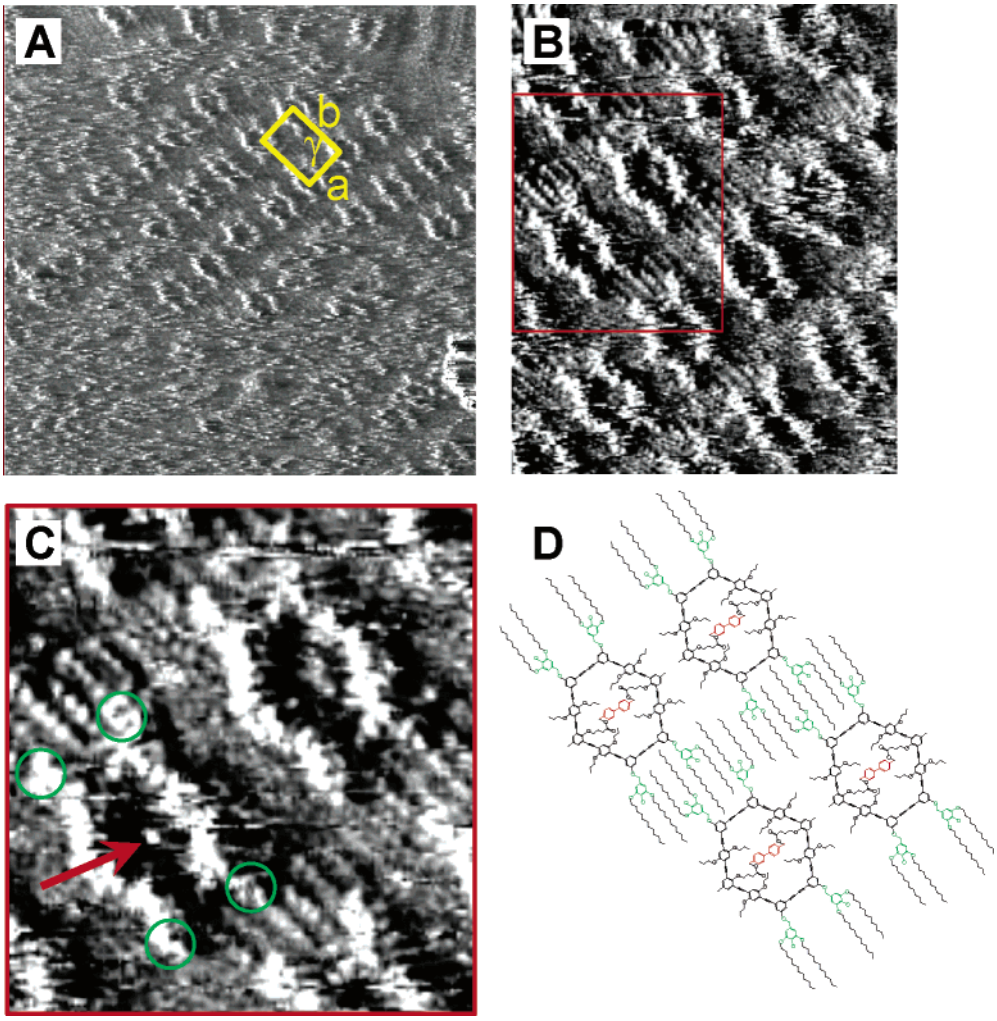


**Figure 2.** Physisorbed monolayer of **16a** at the 1-phenyloctane/graphite interface. (A) 37 × 37 nm$^2$; $I_t$ = 1.00 nA; $V_{bias}$ = −0.508 V. The rectangular unit cell is indicated in yellow. (B) 16.3 × 16.3 nm$^2$; $I_t$ = 1.00 nA; $V_{bias}$ = −0.508 V. (C) A zoom-in image of the area indicated in part B (10 × 10 nm$^2$). The tentative location of the biphenylene bridge is indicated with a red arrow, and the four extraannular groups are indicated with green circles. (D) Molecular model: the biphenylene bridge is indicated in red, the four extraannular groups are in green, and the visible alkyl chains are in black.

to fill the empty interior of adjacent rings prevents the formation of a stable liquid crystalline phase. In contrast to **1**, **2a** and **2b** form a columnar mesophase over a broad temperature range: here, the inside of the molecules is filled by the ester groups which preclude the conflict described above. Independent investigations on other shape-persistent macrocycles with fixed intraannular alkyl chains support this hypothesis.[16] The observation of a mesophase in **2** has additionally shown that the size balance between the rigid core and the flexible periphery in these rings is correct and allows the observation of an ordered fluid phase in these molecules.[21] Accordingly, we expected also the existence of a thermotropic mesophase for **16a** and **16b**. Moreover, the biphenylene core inside the macrocycles **16** may even broaden the temperature range of the columnar mesophase compared to **2** because **16** contains an additional aromatic $\pi$ system.[22,23] However, investigations of the thermal behavior of **16a** and **16b** showed that this is not the case. **16a** has a sharp melting point of 148−149 °C, while **16b** has a broader melting regime. It softens slightly below 100 °C and melts completely at 114−116 °C. Both compounds melt isotropically, and also quenching of the isotropic phase gave no indication for the formation of a mesophase in either case. Although at first glance this is surprising, the absence of a mesophase could be explained by the size and conformation of the intraannular filling of **16**. Simple CPK models indicated that the template and its connectors to the macrocycle (i.e., the biphenylene bridge) are longer than the diameter of the ring. Accordingly, **16a** and **16b** can be viewed as macrocycles with a loop that prevents a planar shape. They seem to have, opposite to **2**, a more spherical shape and do not form a mesophase. Because an X-ray structure of **16a** or **16b** is not available, we turned to the STM investigations which became now even more important because they may also provide insight into the conformation of the macrocycles.

**Adsorption on the Graphite Surface.** The strong influence of the biphenylene bridge on the thermal behavior of the macrocycles suggests that the adsorption behavior of **16** on solid substrates may also differ from that of macrocycles **1** and **2**. The two-dimensional self-assembly of macrocycles

(21) Kohnke, B.; Praefke, K. *Chem.-Ztg.* **1985**, *109*, 121−127.
(22) Collings, P. J.; Hird, M. *Introduction to Liquid Crystals*; Taylor & Francis, Ltd.: London, 1997; p 83.
(23) Ultimately, the biphenylene core in **16** might be replaced by a condensed polycyclic aromatic hydrocarbon leading to a new design for electronically active $\pi$ systems.

**16** on graphite was investigated at the liquid/solid interface. The nature of the interaction with the substrate is physisorption, and STM is the technique of choice to obtain detailed information on the ordering and structural aspects of the adsorbed molecules with submolecular resolution,[24] including macrocycles.[4,6−8] The compounds were dissolved in 1-phenyloctane or TCB, and a drop of the solution was brought onto a freshly cleaved surface of HOPG. Some representative STM images of well-ordered monolayers of **16a** formed at the 1-phenyloctane/graphite interface are shown in Figure 2. On a local scale (e.g., the upper right part of Figure 2A), regular patterns are observed. In the other part of that image, the lack of order is most likely caused by the mobility of the molecules. In the STM images, the bright ringlike structures (high tunneling current) are attributed to the unsaturated backbone of the shape-persistent macrocycles, because the energy difference between the frontier orbitals and the Fermi level of the graphite is rather small.[25] Additionally, the contrast within a macrocycle correlates with the density of the highest occupied molecular orbital (HOMO) of the ring, as we have reported earlier.[6] The four extraannular groups with oligo-alkyl side chains are clearly visible and are indicated with green circles. The unit cell parameters were determined to be $a = 3.9 \pm 0.1$ nm, $b = 5.1 \pm 0.1$ nm, and $\gamma = 90 \pm 1°$. The occupied area per molecule is similar to the values obtained for **1** and **2a** on graphite and shows that the lattice parameters are dominated by the rigid macrocycle and the alkyl periphery and are only marginally influenced by the ring interior. The diameters of the macrocycles along the unit cell vectors *a* and *b* are 2.6 ± 0.2 nm and 2.5 ± 0.1 nm, respectively. These data also correspond well with the molecular dimensions of the similar macrocycles obtained by single-crystal X-ray analysis.[2a] The alkyl chains are located between adjacent rows of the macrocycles and are interdigitated. They run parallel with one of the main symmetry axes of graphite underneath the monolayer, revealing the interaction between the alkyl chains and the substrate. The alkyl chains run almost perpendicular to the macrocycle rows. According to the analysis, at least one alkyl chain per extraannular group along the unit cell vector *b* is either directed to the liquid phase or adsorbed in a disordered fashion between the macrocycles along unit cell vector *a*. Therefore, that alkyl group is not visible in the STM images. Figure 2D is a molecular model illustrating the orientation of individual macrocycles and their alkyl chains.

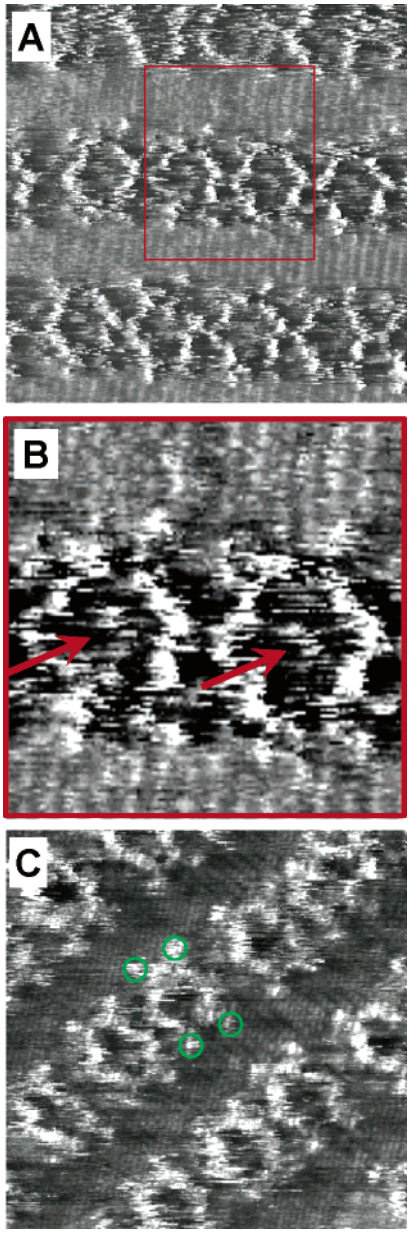


**Figure 3.** Physisorbed monolayer of **16b** at the TCB/graphite interface. (A) 14.1 × 14.1 nm$^2$; $I_t = 0.6$ nA; $V_{bias} = -0.484$ V. (B) A zoom-in of the area indicated in red in part A (10 × 10 nm$^2$). (C) 27.5 × 27.5 nm$^2$; $I_t = 0.6$ nA; $V_{bias} = -0.370$ V. The apparent location of the biphenylene bridge is indicated by a red arrow, and the extraannular groups are indicated by green circles.

(24) (a) Foster, J. S.; Frommer, J. E. *Nature* **1988**, *333*, 542−545. (b) Rabe, J.; Buchholz, S. *Science* **1991**, *253*, 424−427. (c) Cyr, D. M.; Venkataraman, B.; Flynn, G. W. *Chem. Mater.* **1996**, *8*, 1600−1615. (d) Giancarlo, L. C.; Flynn, G. W. *Annu. Rev. Phys. Chem.* **1998**, *49*, 297−336. (e) De Feyter, S.; Gesquière, A.; Abdel-Mottaleb, M. M.; Grim, P. C. M.; De Schryver, F. C.; Meiners, C.; Sieffert, M.; Valiyaveettil, S.; Müllen, K. *Acc. Chem. Res.* **2000**, *33*, 520−531. (f) Samori, P.; Yin, X.; Tchebotareva, N.; Wang, Z.; Pakula, T.; Jäckel, F.; Watson, M. D.; Venturini, A.; Müllen, K.; Rabe, J. P. *J. Am. Chem. Soc.* **2004**, *126*, 3567−3575. (g) Claypool, C.-L.; Faglioni, F.; Goddard, W. A.; Gray, H. B.; Lewis, N. S.; Marcus, R. A. *J. Phys. Chem. A* **1997**, *101*, 5978. (h) Griessl, S.; Lackinger, M.; Edelwirth, M.; Hietschold, M.; Heckl, W. M. *Single Mol.* **2002**, *3*, 25. (i) Pan, G.-B.; Liu, J.-M.; Zhang, H.-M.; Wan, L.-J.; Zheng, Q.-Y.; Bai, C.-L. *Angew. Chem.* **2003**, *115*, 2853−2857; *Angew. Chem., Int. Ed.* **2003**, *42*, 2747−2751. (j) Yoshimoto, S.; Tsutsumi, E.; Honda, Y.; Murata, Y.; Murata, M.; Komatsu, K.; Ito, O.; Itaya, K. *Angew. Chem.* **2004**, *116*, 3106−3109; *Angew. Chem., Int. Ed.* **2004**, *43*, 3044−3047. (k) Safarowsky, C.; Merz, L.; Rang, A.; Broekmann, P.; Hermann, B. A.; Schalley, C. A. *Angew. Chem.* **2004**, *116*, 1311−1314; *Angew. Chem., Int. Ed.* **2004**, *43*, 1291−1294. (l) Safarowsky, C.; Wandelt, K.; Broekmann, P. *Langmuir* **2004**, *20*, 8261−8269. (m) Cai, Y. G.; Bernasek, S. L. *J. Am. Chem. Soc.* **2004**, *126*, 14234−14238. (n) Chang, S. *Chem. Rev.* **1997**, *97*, 1083−1096. (o) Barlow, S. M.; Raval, R. *Surf. Sci. Rep.* **2003**, *50*, 201−341. (p) Rosei, F.; Schunack, M.; Naitoh, Y.; Jiang, P.; Gourdon, A.; Laegsgaard, E.; Stensgaard, I.; Joachim, C.; Besenbacher, F. *Prog. Surf. Sci.* **2003**, *71*, 95−146. (q) Böhringer, M.; Morgenstern, K.; Schneider, W.-D.; Berndt, R. *Angew. Chem.* **1999**, *111*, 832−834; *Angew. Chem., Int. Ed.* **1999**, *38*, 821−823. (r) Spillmann, H.; Dmitriev, A.; Lin, N.; Messina, P.; Barth, J. V.; Kern, K. *J. Am. Chem. Soc.* **2003**, *125*, 10725−10728. (s) de Wild, M.; Berner, S.; Suzuki, H.; Yanagi, H.; Schmettwein, D.; Ivan, S.; Baratoff, A.; Guentherodt, H.-J.; Jung, T. A. *ChemPhysChem* **2002**, *10*, 881−885. (t) Theobald, A.; Oxtoby, N. S.; Phillips, M.; Champness, N. R.; Beton, P. H. *Nature* **2003**, *424*, 1029−1031. (u) Hipps, K. W.; Scudiero, L.; Barlow, D. E.; Cooke, M. P., Jr. *J. Am. Chem. Soc.* **2002**, *124*, 2126−2127.

(25) Lazzaroni, R.; Calderone, A.; Brédas, J. L.; Rabe, J. P. *J. Chem. Phys.* **1997**, *107*, 99−105.

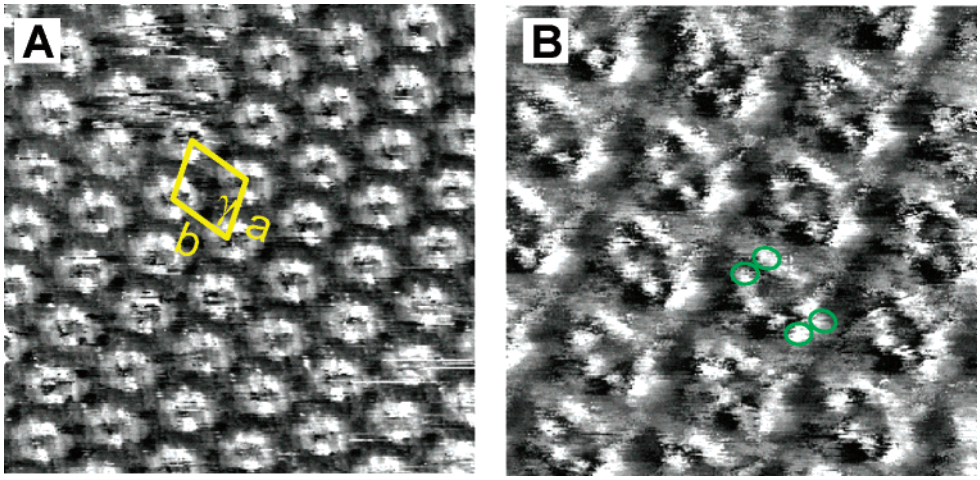


**Figure 4.** STM images of **16a** at the TCB/graphite interface. **(**A) 29.6 × 29.6 nm$^2$; $I_t$ = 0.55 nA; $V_{bias}$ = −1.612 V. The oblique unit cell is indicated in yellow. (B) 16.9 × 16.9 nm$^2$; $I_t$ = 0.5 nA; $V_{bias}$ = −1.584 V. The four extraannular groups are indicated with green circles.

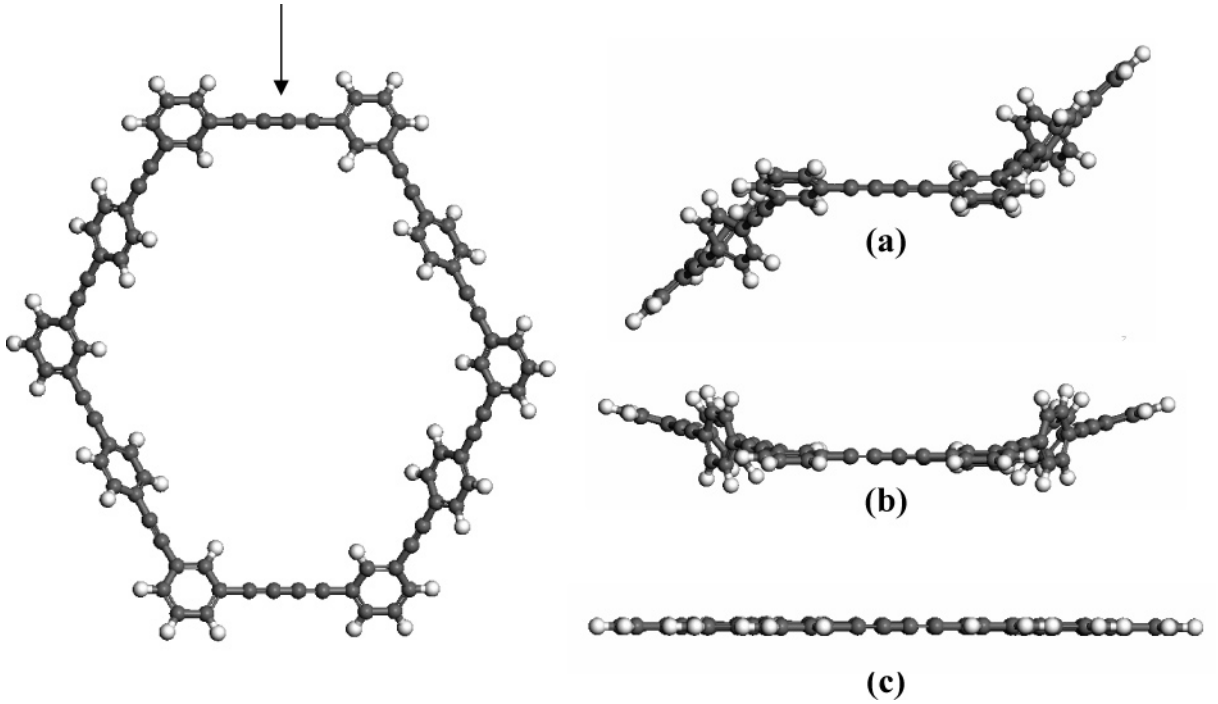


**Figure 5.** Conformations of the phenylene−ethynylene core. Left: the most stable conformation, i.e., the "chair" conformation. Right: the different conformations, as viewed along the direction shown by the arrow on the left. (a) The "chair" conformation, Δ = 0 kcal/mol (by definition). (b) The "boat" conformation, Δ = 4.2 kcal/mol. (c) The "flat" conformation, Δ = 9.9 kcal/mol.

Similar conclusions can be drawn for the C16 analogue **16b** physisorbed at the TCB/graphite interface (Figure 3). Difficulties in recording the graphite substrate underneath the monolayer prevented an accurate unit cell determination. Nevertheless, qualitatively the same ordering was observed as for **16a** at the l-phenyloctane/solid interface.

The two-dimensional self-assembly of **16a** at the TCB/HOPG interface revealed a different packing (Figure 4). Individual macrocycles can clearly be distinguished whereas the alkyl chains cannot be imaged. The tentative location of the four extraannular phenyl rings bearing the alkyl chains is indicated with green circles. The unit cell parameters were determined to be $a = 4.4 \pm 0.1$ nm, $b = 4.5 \pm 0.1$ nm, and $\gamma = 70 \pm 1°$. Although the resolution is less compared to the images obtained for those monolayers physisorbed from 1-phenyloctane, the degree of long-range ordering is more pronounced. Interestingly, the same observation was made for **2a** when monitoring its self-assembly in these solvents.[7] This observation supports our assumption that the main reason for the lack of long-range order is a very sensitive interplay between kinetically and thermodynamically controlled monolayer formation. Compounds **1**, **2**, and **16** contain 12 long alkyl chains that lead to a considerable interaction with the graphite substrate (additionally to the interaction between the aromatic rings parts and the substrate). Therefore, the molecules are immobilized at the graphite although they are not packed in an ideal fashion (kinetically trapped). In TCB, which is a better solvent for these macrocycles, the extent of kinetic trapping will be less, leading to more long-range ordered structures. Although difficult to quantify, the degree of ordering for both macrocycles **16a** and **16b** is higher than for the analogue compounds **2a** and **2b**. At

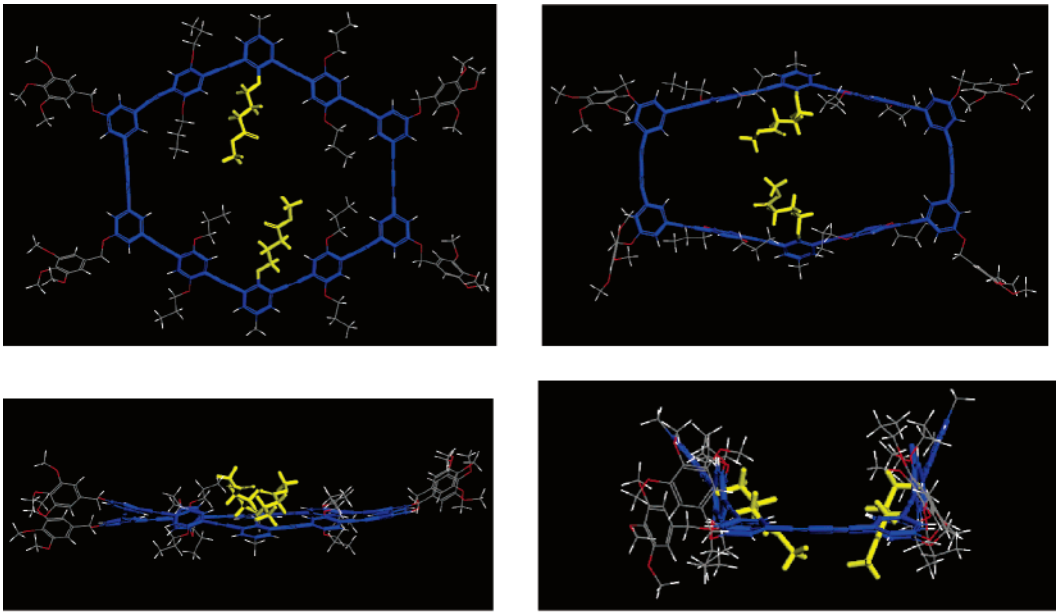


**Figure 6.** Specific conformations of the macrocycle **2′**: (a) the "flat" conformation and (b) the "boat" conformation. Top and bottom views are shown with the core face-on and edge-on to the view, respectively.

present, we interpret this as a consequence of a lower degree of "kinetic trapping". In other words, **16a** and **16b** are not as strongly adsorbed at the graphite surface as **2a** and **2b** and are, therefore, able to self-assemble in a more ideal fashion.

As indicated by red arrows in the respective STM images (Figure 2C and Figure 3B), sometimes a bright feature is visible inside the macrocycle, which might indicate the location of the biphenylene bridge. As discussed above, the probability of finding the biphenylene group in the plane of the macrocycle should be rather low, and we expect it to be located above the macrocycle ring. However, if the biphenylene group is not in contact with the substrate, electronic coupling with the HOPG is small and electron tunneling "through" these groups will be limited.[26] Therefore, the observation of the biphenylene bridge in the STM images is somewhat surprising and seems to be contradictory with the thermal behavior of these compounds. Subsequently, molecular modeling studies were performed to understand the conformational behavior of the molecules in more detail.

**Molecular Modeling.** To understand the impact of the intraannular biphenylene bridge on the conformation of the macrocycle, simulations of model compounds for **2** and **16** were performed. To keep the computational effort to a reasonable level, the long chains at the periphery of the compounds were replaced by methyl groups. Therefore, those model systems were referred as **2′** and **16′**, respectively.

As a preliminary step, molecular mechanics (MM) simulations on the unsubstituted ring were carried out (Figure 5), obtaining well-defined energy minima due to inter-ring torsions. The most stable conformer is the "chair" structure (defined as $\Delta = 0$ kcal/mol, see Figure 5). In this conformation, the torsion angle between atoms 1−2−3−4 (see labeled carbons in Chart 3) is −29.2°. The "boat" conformation (Figure 5b), with a torsion angle 1−2−3−4 of ±14.9°, is less stable by 4.2 kcal/mol. Note that several other "chair" structures with energies lying between the most stable configuration and the "boat" configuration have also been found. The least stable of the depicted conformations is the "flat" one (torsion angle 1−2−3−4 of 0.0°), which is nearly 10 kcal/mol less stable than the "chair" conformation. These results are in line with previous simulations,[6] which have also shown these structures as stable conformers of a macrocycle with no intraannular bridge group.

**Chart 3**

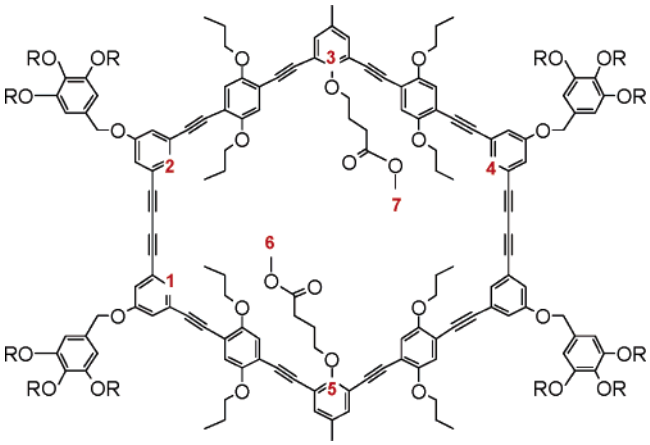


In the second stage of the modeling, ester-type macrocycle **2′** (Chart 3) was investigated starting from a MM-optimized "flat" conformation (Figure 6a): the core is nearly planar (torsion angle 1−2−3−4 of 7°), with distances 2−4 and 3−5 of 21.9 and 19.5 Å, respectively. This conformation is similar to the planar structure of the unsubstituted phenylene−ethynylene core. Applying a MD simulation allows the system to evolve toward more stable conformations, such

(26) (a) Jung, T. A.; Schlittler, R. R.; Gimzewski, J. K.; Tang, H.; Joachim, C. *Science* **1996**, *271*, 181−184. (b) Jung, T. A.; Schlittler, R. R.; Gimzewski, J. K. *Nature* **1997**, *386*, 696−698.

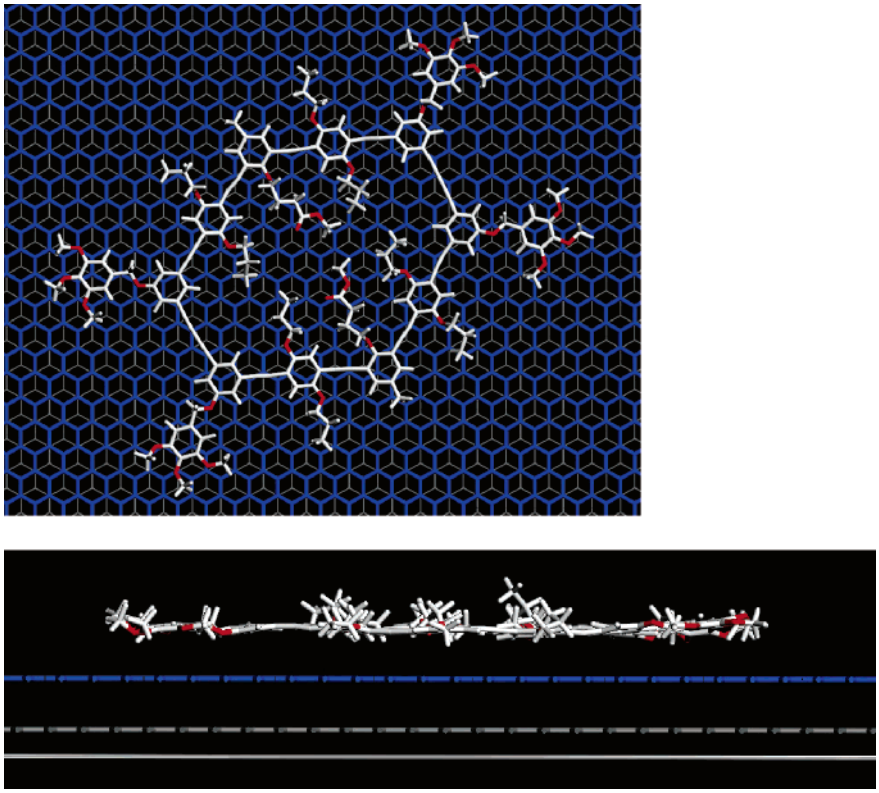

**Figure 7.** Top and side views of the stable conformation of **2′** on graphite from a combined MD + MM simulation.

as that shown in Figure 6b, and it corresponds to a "boat" structure. In this conformation, the torsion angle 1−2−3−4 is around 42°, while for the "boat" structure of the unsubstituted macrocycle (Figure 5) it is only around 15°. This difference is likely due to the interaction appearing between the intraannular ester groups in the "boat" conformation (in yellow in Figure 6b); the shortest contact between the two group is 2.9 Å, while it is 5.0 Å for the "flat" conformation shown in Figure 6a. Consequently, the distance 2−4 in the "boat" conformation is larger than in the "flat" conformation (23.5 vs 21.9 Å) while the distance 3−5 in the "boat" conformation is shorter (13.5 vs 19.5 Å). The interaction between the intraannular ester groups stabilizes the electrostatic and van der Waals energies of the "boat" conformation by 9.0 kcal/mol compared to the "flat" one, while the internal energy is higher by 2.6 kcal/mol (due to the strong torsion). Globally, the "boat" conformation is, thus, 6.4 kcal/mol more stable than the "flat" conformation. Note that several stable chair conformations have also been found, but they appear to be less stable than the "boat" structure (in contrast to the situation in the phenylene−ethynylene core alone) because they lack the favorable interactions that are present between the intraannular groups in the "boat" conformation of **2′**.

Starting from both the "flat" and the "boat" conformations of **2′** and applying a MM procedure for the adsorption on graphite leads to the planarization of the core at an equilibrium distance of around 3.5 Å to the graphite sheet. When applying a MD simulation, the core stays planar, parallel to the graphite sheet, as shown in Figure 7. The distance 2−4 remains almost constant during the whole MD run (200 ps), with a value oscillating between 21 and 22 Å. In Figure 7, the ester-containing intraannular groups are adsorbed parallel to the graphite, in an extended configuration (the distance

**Chart 4**

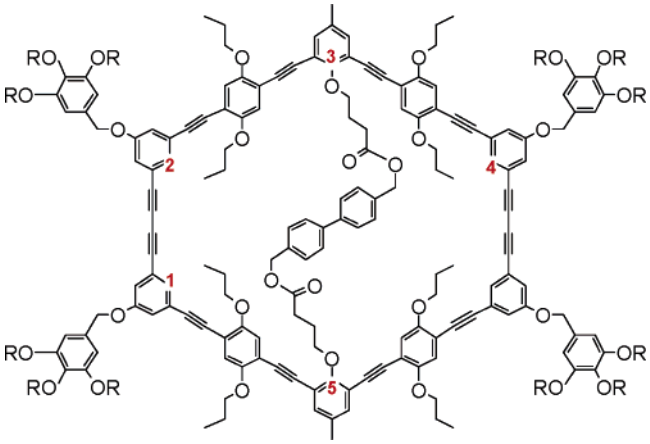


6−7 is around 3.5 Å). These groups show a moderate mobility in the *c* direction (i.e., perpendicular to the graphite plane): for an atom of the ester group, the self-diffusion constant *D* is on the order of $0.6 \times 10^{-2}$ Å$^2$/(ps·atom), larger than that of the atoms of the core, for which the distance to the graphite plane remains basically constant [$D = 0.3 \times 10^{-4}$ Å$^2$/(ps·atom)].[27]

MM simulations on **16′** (Chart 4) starting from a "flat" macrocycle show that the presence of the bridge greatly affects the core planarity. The conformation shown in Figure 8a, where the bridge adopts a "U-shape" conformation, is

(27) The self-diffusion constant of an atom or a group of atoms can be evaluated from the mean-square displacement during the MD run and is defined as

$$D = \frac{1}{6N} \lim_{t\to\infty} \frac{d}{dt} \sum_{i=1}^{N} \langle [r_i(t) - r_i(0)]^2 \rangle,$$

where *t* is the dynamics time and *N* is the number of atoms.

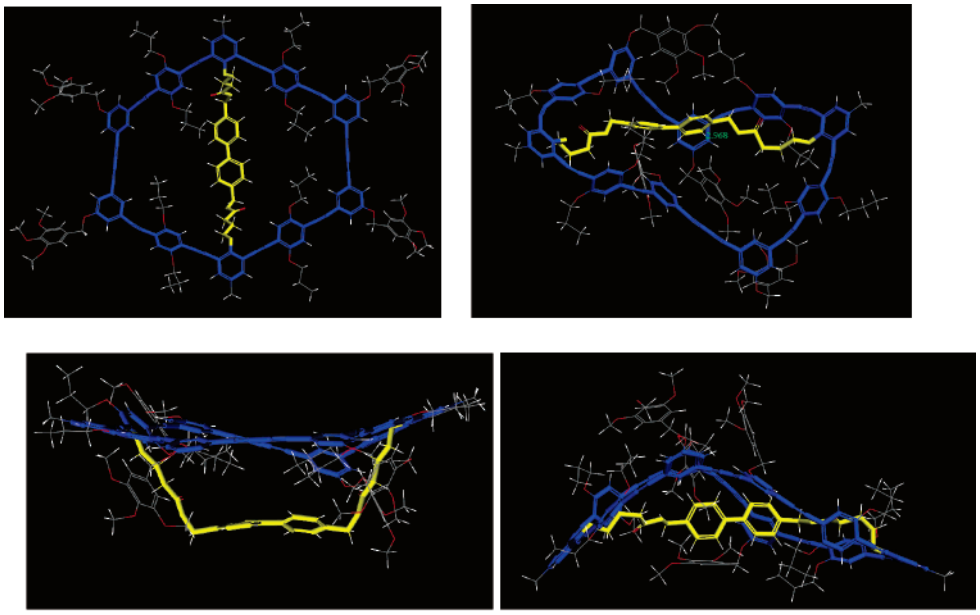


**Figure 8.** Specific conformations of the macrocycle **16′**: (a) the "U-bridge" structure, with a slightly bent core (blue) and a "U"-shaped bridge (yellow) and (b) the "folded" structure, with a $\pi$ complex between the bridge (yellow) and the core (blue). Top and bottom views are shown with the core face-on and edge-on to the view, respectively.

the result of this simulation. The subsequent MD simulation reveals much more conformational freedom than for the core alone: the presence of the eight alkoxy chains and the bridge strongly modifies the potential energy surface by introducing numerous possibilities of attractive nonbonded interactions between the core and the intraannular groups. In particular, the core tends to fold as a result of the possibility to form a $\pi$ complex with the biphenyl part of the bridge, which generates a very stable conformation that is maintained over the whole MD trajectory (see the "folded" conformation in Figure 8b). The formation of this $\pi$ complex globally decreases the energy of the system and stabilizes it by about 25 kcal/mol (via van der Waals interactions) compared to the "U-bridge", even though the overall internal energy of the molecule increases by 5 kcal/mol, as a result of the large torsion angles between phenyl rings of the core. The "folded" structure is, therefore, more stable by about 20 kcal/mol, compared to the "U-bridge" conformation. The $\pi$ complex between a phenyl ring of the core and a phenyl ring of the bridge is characterized by a nearly T-shaped conformation of the interacting aromatics, reminiscent of the conformation of the benzene dimer. The torsion angle between the two phenyl rings in the center of the bridge (though alternating during the simulation) has an absolute value around 23−24° in both configurations in Figure 8. Note that because the length of the fully extended biphenylene bridge is larger than the size of the cavity (i.e., the distance 3−5), the macrocycle strongly deforms. The distance 2−4 stabilizes at around 14−15 Å when the $\pi$ complex is formed (from an initial value around 21 Å), while the distance 3−5 evolves from 18.3 Å (in the "U-bridge" structure) to around 23 Å (in the "folded structure").

These calculations indicate that the stable conformations of **16′** as an isolated molecule are very likely those with an intramolecular $\pi$ complex between the bridge and the core. Note, however, that the calculations do not take into account the influence of a solvent, which can have a strong influence on the conformations of the macrocycle:[2c] good polar solvents could hinder the formation of the intramolecular $\pi$ complex by specific interactions with the ester groups of the bridge.

Both conformations shown in Figure 8 have been used as input for simulations of the adsorption on graphite. Starting from the U-bridge conformation, the core is found to be parallel and strongly interacting with graphite, at a distance of around 3.5 Å from the surface. This distance remains almost constant during the whole MD simulation. In strong contrast with the macrocycle in a vacuum, the core does not tend to fold during the MD to form a $\pi$ complex with the bridge. On graphite the core stays planar, which highlights the strong interaction between the core and this substrate. Therefore, the distance 2−4 remains large, and around 21−22 Å along the whole MD run during the simulation, the bridge is quite flexible and interacts alternatively with the graphite via its different segments (the two saturated groups and the biphenyl central part). In terms of comparison of "mobility" in the *c* direction (perpendicular to the plane of the graphite), the self-diffusion constant *D* for atom 3 (Chart 4) is on the order of $0.3 \times 10^{-4}$ Å$^2$/(ps·atom) (i.e., there is almost no change in the distance to the graphite plane), while for an atom in the biphenyl bond, it is on the order of $0.2 \times 10^{-1}$ Å$^2$/(ps·atom). The latter value reflects significant mobility in this direction, one order of magnitude larger than for the intraannular groups in **2′**. One of the most stable conformations of adsorbed **16′** is shown in Figure 9. In this structure, the biphenyl part of the bridge is interacting with the graphite. It is located at a distance between 3.5 and 4.0 Å and oriented almost parallel to the graphite, with a torsion

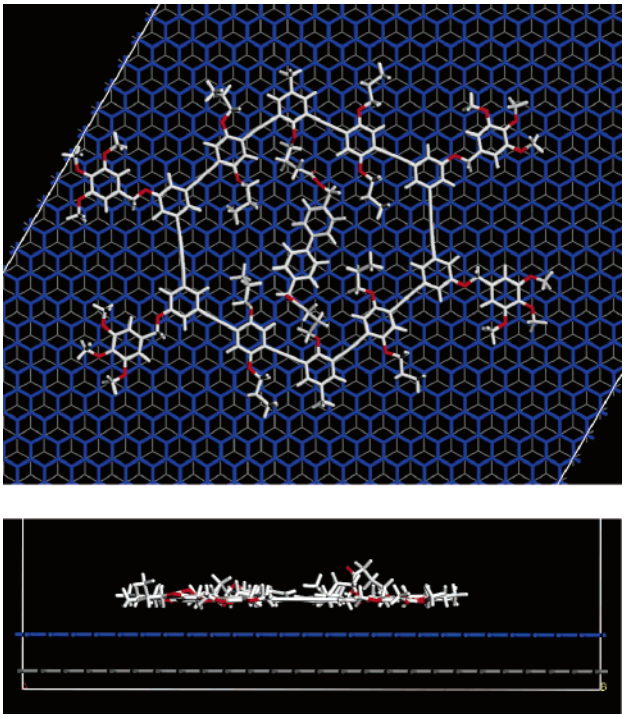

**Figure 9.** Top and side views of the stable conformation of **16′** on graphite from MD + MM simulations starting from the "U-bridge" conformation.

angle between the benzene rings of 24°. Because the length of the fully extended bridge is larger than the distance 3−5, one of the ester groups is not parallel to the graphite but pointing away from the surface. Note that the eight propoxy groups (four intraannular and four extraannular) as well as the tolyl groups are parallel to the graphite surface, at the same distance as the core.

The same approach was applied to simulate the adsorption of the "folded" macrocycle on graphite. During the MD simulation, the shape of the molecule changes dramatically: the macrocycle tends to unfold to maximize the interactions between the core and the graphite. This is illustrated by the change in the distance 2−4: starting at a value of about 14 Å, this distance evolves rapidly during the initial stages of the simulation until reaching an equilibrium value of 21−22 Å. This is the same distance as for the macrocycle adsorbed from the "U-bridge" configuration. This unfolding of the macrocycle on graphite is due to the tendency of the conjugated core to interact with this surface and is, therefore, accompanied by a very large stabilization by van der Waals interactions. These results highlight the fact that, whatever the initial geometry of the molecule, the conjugated core tends to unfold upon adsorption on graphite and becomes planar to maximize the interaction with the substrate.[28]

The comparison between the simulations of the phenylene−ethynylene core and the model systems **2′** and **16′** in a vacuum clearly shows that the intraannular groups have a strong influence on the "conformational landscape" of the molecules. For the unsubstituted macrocyle (Figure 5), the distances 2−4 and 3−5 are almost identical for all the possible conformations (chair, boat, flat), highlighting the rigidity of the core. With nonbridged intraannular ester groups (**2′**) the boat conformation with a larger 2−4 distance and a shorter 3−5 distance becomes more stable by 6.4 kcal/mol over the flat conformation. Even more distorted from planarity is the bridged macrocycle **16′** which tends to fold with a bent core, giving rise to $\pi-\pi$ interactions between the biphenyl part of the bridge and the ring. On graphite, regardless of the starting conformation of the macrocycles, the molecules tend to unfold, flatten upon adsorption, and maximize the interactions between the core and the surface. Although the biphenylene bridge of **16′** is longer than the diameter of the ring, the biphenylene part can interact with the graphite and indeed be in the ring plane. However, the mobility of the biphenylene bridge along the *c* direction is much higher than the mobility of the ester groups in **2′**. Additionally, when the biphenylene bridge is in contact with the graphite, one of the ester groups points away from the surface. Although the calculations on the isolated molecules describe the gas phase conformation, the results are useful to explain two experimental observations that seem to be contradictory: (1) the absence of a mesophase and the melting direct into an isotropic phase, which suggests that the presence of the intraannular biphenylene bridge leads to a bulky core structure for macrocycle **16**, and (2) the "flat" appearance of the macrocycle (sometimes including the visualization of the biphenylene bridge) in the STM images, suggesting a rather planar conformation of macrocycle **16**. The calculations clearly point to a major conformational change of the macrocycle to a planar structure upon adsorption, which appears to reconcile the experimental observations.

## Conclusion

In summary, we have presented the synthesis of shape-persistent macrocycles **16** with extraannular oligo-alkyl side chains and an intraannular bis(hydroxymethyl)biphenylene diester group. The preparation of the ring is based on a template-supported cyclization giving the macrocycle in 81% yield. The intraannular filling of the compounds in combination with the oligo-alkyl side groups should enable the materials to melt into a liquid crystalline phase, as it is also observed for **2**. However, because the template is longer than the diameter of the rings, the formation of the loop precludes the mesophase formation. We also investigated the adsorption of **16** from solution onto the surface of HOPG. The long-range order of the molecules and the image resolution is influenced by the side groups and the solvent used for the self-assembly. With more polar solvents (TCB vs 1-phenyloctane) a better ordering of the molecules is observed, although not ideal. Qualitatively the ordering of **16** is better than for **2**. This shows that the loop of the biphenylene bridge influences the adsorption/desorption equilibrium such that an irregular, kinetic trapping of the molecules is reduced. As a result, submolecular resolution is possible and allows sometimes the recognition of the intraannular biphenylene bridge. This can only be explained if the biphenylene is also adsorbed at the graphite. Although this seems to be contradictory to the fact that the bridge is longer than the ring diameter, MM and MD calculations show that the rings

(28) It should be noted that a folded structure on graphite (extracted from MD with subsequent MM) is about 30 kcal/mol less stable than the conformation shown in Figure 9.

(including the bridge) have a strong tendency to flatten upon the adsorption process. For future templating and complexation purposes, insight into the conformational changes upon adsorption is crucial.

## Experimental Procedures

**Synthesis.** Reactions requiring an inert gas atmosphere were conducted under argon, and the glassware was oven-dried (140 °C). THF was distilled from potassium prior to use. Triethylamine, piperidine, and pyridine were distilled over $CaH_2$ and stored under argon. Commercially available chemicals were used as received. $^1$H NMR solution spectra were recorded on a Bruker DPX 250 or AC 300 spectrometer (250 and 300 MHz for $^1$H, 62.5 and 75.48 MHz for $^{13}$C). Chemical shifts are given in parts per million, referenced to residual proton resonances of the solvents. Thin-layer chromatography was performed on aluminum plates precoated with Merck 5735 silica gel 60 $F_{254}$. Column chromatography was performed with Merck silica gel 60 (230 ± 400 mesh). The gel permeation chromatograms were measured in THF (flow rate 1 mL $min^{-1}$) at room temperature, using a combination of three styragel columns (porosities $10^3$, $10^5$, $10^6$) and an UV detector operating at $\lambda = 254$ nm. The molecular weight was obtained from polystyrene calibrated size-exclusion chromatography columns. The MALDI-TOF mass spectroscopy measurements were carried out on a Bruker reflex spectrometer (Bruker, Bremen), which incorporates a 337-nm nitrogen laser with a 3-ns pulse duration ($10^6 \pm 10^7$ W/cm, 100-mm spot diameter). The instrument was operated in a linear mode with an accelerating potential of 33.65 kV. The mass scale was calibrated with polystyrene ($M_p = 2300$), using a number of resolved oligomers. Samples were prepared by dissolving the macrocycle in THF at a concentration of $10^{-4}$ mol/L. In all cases, 1,8,9-trihydroxyanthracene (Aldrich, Steinheim) was used as the matrix. In general, silver trifluoroacetate was added to the samples. Field desorption spectra were recorded on a VG ZAB 2-SE FPD machine.

**STM.** STM experiments were performed using a Discoverer scanning tunneling microscope (Topometrix, Inc., Santa Barbara, CA) along with an external pulse/function generator (model HP 8111 A), with negative sample bias. The tips were electrochemically etched from Pt/Ir wire (80%/20%, diameter 0.2 mm) in a 2 N KOH/6 N NaCN solution in water. Prior to imaging, all compounds under investigation were dissolved in 1-phenyloctane (Aldrich 99%) and TCB (Aldrich 99%) at a concentration of approximately 1 mg/g, and a drop of the solution was applied onto a freshly cleaved surface of HOPG (grade ZYB, Advanced Ceramics, Inc., Cleveland, OH). Then, the STM tip was immersed in the solution and images were recorded at the liquid−solid interface. The STM images were acquired in the variable-current mode (constant height). The measured tunneling currents are converted into a gray scale: black (white) refers to a low (high) measured tunneling current. The experiments were repeated in several sessions using several tips to check for reproducibility and to avoid artifacts. For analysis purposes, recording of a monolayer image was followed by imaging the graphite substrate underneath under the same experimental conditions, except for the lowered bias voltage. Before image analysis, the images were corrected for drift, via scanning probe image processor (SPIP) software (Image Metrology ApS), using the recorded graphite images for calibration. However, for display purposes, the images shown are not corrected for scanner drift. The imaging parameters are indicated in the figure captions: tunneling current ($I_t$) and sample bias ($V_{bias}$).

**Calculations.** Simulations have been performed using the Materials Studio 3.0 package from Accelrys. The COMPASS force field[29] was used for the calculations as it provides an accurate description of the geometry and the torsional barriers of phenylene−ethynylene oligomers and saturated chains such as alkoxy or alkyl chains. For the simulation of a single molecule in a vacuum, the core was first built planar and a preliminary MM minimization was performed. The nonbonded van der Waals and electrostatic terms are described using a Spline function, with a cutoff of 14.0 Å (spline width: 3 Å). The root-mean-square force convergence parameter is set to $10^{-3}$ kcal/(mol·Å). A MD procedure was then applied to the system using the canonical ensemble (*N*, *V*, *T*) at 298 K using the Nosé−Hoover thermostat. The time step is set to 1 fs and the duration of the run is 500 ps, with an output frame every 200 fs. A few minima of the potential energy during the whole MD run were picked from the trajectory file, and a final MM procedure was applied to those structures. For simulating the adsorption of the macrocycle on graphite, periodic boundary conditions were used, with a supercell of two sheets of graphite of 25 × 25 unit cells along the *a* and *b* directions (61.50 × 61.50 Å$^2$) and a vacuum slab of 50.00 Å along the *c* direction. Periodic limit conditions have been set to avoid boundary artifacts. The positions of the atoms of graphite have been kept fixed, because physisorption is not expected to alter the structure of the substrate. The macrocycle was inserted into the periodic lattice at a distance of 6.0 Å of the first graphitic layer, and the adsorption was simulated by preliminary MM calculations. A MD procedure of 200 ps was then performed, with the same methodology as for the single molecule in a vacuum (output frame every 125 fs). Subsequent MM calculations of few MD potential energy minima were carried out to find the most stable configurations. For those simulations, the nonbonded electrostatic terms are described using the Ewald technique for periodic systems (accuracy of 0.01 kcal/mol), while van der Waals interactions were described with atom-based interactions using a Spline function (cutoff 14 Å).

**Methyl 4-(2,6-Diiodo-4-methylphenoxy)butanoate (4).**[7] 4-Methyl-2,6-diiodophenol (**3**; 7.90 g, 22.0 mmol), 4-bromotrimethylorthobutyrate (5.0 g, 22.0 mmol), $K_2CO_3$ (3.0 g, 21.7 mmol), and KI (50 mg) were stirred in dimethylformamide (DMF; 35 mL) at 60 °C for 48 h and after cooling to room temperature poured into ether and water. The organic phase was separated and extracted with water, 10% acetic acid, water, 10% aqueous sodium hydroxide, water, and brine. After drying over $MgSO_4$ and evaporation of the solvent the crude product was chromatographed over silica gel with $CH_2Cl_2$/petroleum ether (PE; 1:4) as the eluent ($R_f = 0.45$) to give **4** as a white solid (8.09 g, 73%). Although the ortho ester hydrolyzes during the workup procedure, the crude product may contain variable minor amounts of the corresponding ortho ester product, seen by an extra NMR signal at 3.19 ppm (s). In that case the crude product was dissolved in $CH_2Cl_2$ and extracted several times with 10% acetic acid, then water, 10% aqueous sodium hydroxide, water, and brine to complete the transformation of the ortho ester to **4**. $^1$H NMR (300 MHz, $CD_2Cl_2$): $\delta = 7.60$ (s, 2 H), 3.96 (t, $J = 5.7$ Hz, 2 H), 3.67 (s, 3 H), 2.66 (t, $J = 7.6$ Hz, 2 H), 2.23 (s, 3 H), 2.12−2.22 (m, 2 H). MS (FD): 459.9 ($M^+$), 920.1 (2 $M^+$).

**Methyl 4-(2,6-Bis{2-[2,5-dipropyloxy-4-(2-triisopropylsilylethynyl)phenyl]ethynyl}-4-methylphenoxy)butanoate (6).**[7] Pd$(PPh_3)_2Cl_2$ (65 mg) and CuI (33 mg) were added to a solution of **4** (1.67 g, 3.63 mmol) and **5** (3.07 g, 7.70 mmol) in triethylamine/THF (10:1; 110 mL). The solution was stirred for 24 h at room temperature, for 1 h heated to 50 °C, and after cooling to room-temperature poured into ether and water. The organic phase was separated and extracted with water, 10% acetic acid, water, 10% aqueous sodium hydroxide, water, and brine. After drying over

(29) (a) Sun, H. *J. Phys. Chem. B* **1998**, *102*, 7338−7364. (b) Rigby, D.; Sun, H.; Eichinger, B. E. *Polym. Int.* **1997**, *44*, 311−330.

$MgSO_4$ and evaporation of the solvent the crude product was chromatographed over silica gel with $CH_2Cl_2$/PE (slow polarity increase from 1:4 to 1:1) as the eluent [$R_f$ ($CH_2Cl_2$/PE, 1:1) = 0.86] to give **6** as a slightly yellow solid (3.18 g, 87%). $^1$H NMR (300 MHz, $CD_2Cl_2$): $\delta$ = 7.29 (s, 2 H), 6.99 (s, 2 H), 6.96 (s, 2 H), 4.36 (t, $J$ = 6.1 Hz, 2 H), 3.96 (m, 8 H), 3.53 (s, 3 H), 2.65 (t, $J$ = 7.6 Hz, 2 H), 2.30 (s, 3 H), 2.11 (m, 2 H), 1.82 (m, 8 H), 1.15 (s, 42 H), 1.06 (m, 12 H). MS (FD): 1000.5 ($M^+$).

**Methyl 4-{2,6-Bis[2-(2,5-dipropyloxy-4-ethynylphenyl)ethynyl]-4-methylphenoxy}butanoate (7).**[7] A 1 M solution of $Bu_4NF$ in THF (12.5 mL, 12.5 mmol) was added to a solution of **6** (3.15 g, 3.15 mmol) in THF (20 mL) and water (0.5 mL). The mixture was stirred for 2 h at room temperature and then poured into ether and water. The organic layer was extracted with water and brine and dried over $MgSO_4$. After evaporation of the solvent the residue was purified by chromatography over silica gel with $CH_2Cl_2$/PE (1:1) as the eluent and subsequently recrystallized from methanol (20 mL) to give **7** as a slightly yellow solid [1.56 g, 74%; $R_f$ ($CH_2Cl_2$/PE, 2:3) = 0.65]. $^1$H NMR (250 MHz, $CD_2Cl_2$): $\delta$ = 7.30 (s, 2 H), 7.03 (s, 2 H), 7.00 (s, 2 H), 4.37 (t, $J$ = 5.7 Hz, 2 H), 3.98 (t, $J$ = 6.5 Hz, 4 H), 3.97 (t, $J$ = 6.5 Hz, 4 H), 3.53 (s, 3 H), 3.40 (s, 2 H), 2.66 (t, $J$ = 7.6 Hz, 2 H), 2.31 (s, 3 H), 2.06−2.17 (m, 2 H), 1.76−1.92 (m, 8 H), 1.07 (t, $J$ = 7.5 Hz, 4 H), 1.06 (t, $J$ = 7.4 Hz, 4 H). MS (FD): 688.2 ($M^+$), 344.2 ($M^{2+}$), 1376.1 (2 $M^+$).

**4-{2,6-Bis[2-(2,5-dipropyloxy-4-ethynylphenyl)ethynyl]-4-methylphenoxy}butanoic Acid (8).** $Bu_4NOH$ (40 wt % in water, 13 mL) was added to a solution of **7** (1.00 g, 1.45 mmol) in THF (13 mL) at room temperature. The mixture was stirred for 3 h at 38 °C. After cooling to room temperature, hydrochloric acid (10%, 13 mL), ether, and water were added. The organic phase was separated, extracted with hydrochloric acid (10%) and brine, and dried over $MgSO_4$. Evaporation of the solvent and digestion of the remaining solid residue with PE yielded **8** as a colorless solid (0.70 g, 72%). $^1$H NMR ($CD_2Cl_2$): $\delta$ = 7.30 (s, 2 H), 7.01 (s, 2 H), 6.99 (s, 2 H), 4.38 (t, $J$ = 5.9 Hz, 2 H), 3.96 (t, $J$ = 6.6 Hz, 4 H), 3.95 (t, $J$ = 6.5 Hz, 4 H), 3.38 (s, 2 H), 2.73 (t, $J$ = 7.6 Hz, 2 H), 2.30 (s, 3 H), 2.11 (q, $J$ = 6.6 Hz, 2 H), 1.92−1.72 (m, 8 H), 1.05 (t, $J$ = 7.3 Hz, 6 H), 1.03 (t, $J$ = 7.3 Hz, 6 H). MS (FD) $m/z$: 674 [$M^+$].

**9.** To a solution of **8** (0.69 g, 1.02 mmol) in dry $CH_2Cl_2$ (35 mL) were added 4,4′-bis(hydroxymethyl)biphenylene (0.11 g, 0.51 mmol), pyridinium-4-tolouenesulfonate (0.64 g, 2.17 mmol), and DIC (0.27 g, 2.17 mmol). After stirring for 3 days at room temperature, the solvent was evaporated and the remaining residue was purified by column chromatography over silica gel using $CH_2Cl_2$ as the eluent ($R_f$ = 0.46). **9** (1.05 g, 99%) was obtained as a colorless solid. $^1$H NMR ($CD_2Cl_2$): $\delta$ = 7.52 (d, $J$ = 8.2 Hz, 2 H), 7.29 d, $J$ = 8.2 Hz, 2 H), 7.29 (s, 4 H), 7.01 (s, 4 H), 6.96 (s, 4 H), 5.01 (s, 4 H), 4.38 (t, $J$ = 5.8 Hz, 4 H), 3.93 (t, $J$ = 6.5 Hz, 8 H), 3.92 (t, $J$ = 6.6 Hz, 8 H), 3.37 (s, 4 H), 2.73 (t, $J$ = 7.6 Hz, 4 H), 2.28 (s, 6 H), 2.13 (q, $J$ = 6.7 Hz, 4 H), 1.89−1.69 (m, 16 H), 1.03 (t, $J$ = 7.4 Hz, 12 H), 1.01 (t, $J$ = 7.4 Hz, 12 H). MS (FD) $m/z$: 1528 [$M^+$].

**10.** To a solution of 3,5-diiodo(tetrahydro-*2H*-pyran-2-yloxy)-benzene[6] (1.00 g, 2.32 mmol) in dry piperidine (10 mL) were added CPDMS acetylene (0.34 g, 2.24 mmol), triphenylphosphine (20 mg), CuI (10 mg), and $(Ph_3P)_2PdCl_2$ (20 mg). The mixture was stirred overnight at room temperature. $CH_2Cl_2$ and water were added, and the organic phase was separated and extracted with 10% aqueous NaOH and brine. After drying over $MgSO_4$ and evaporation of the solvent, the remaining residue was purified by column chromatography over silica gel using $CH_2Cl_2$/PE (3:1) as the eluent ($R_f$ = 0.33). **10** (0.45 g, 43%) was obtained as a colorless oil. $^1$H NMR ($CD_2Cl_2$): $\delta$ = 7.43−7.40 (m, 1 H), 7.40−7.36 (m, 1 H), 7.11−7.07 (m, 1 H), 5.37 (t, $J$ = 2.8 Hz, 1 H), 3.85−3.73 (m, 1 H), 3.62−3.52 (m, 1 H), 2.41 (t, $J$ = 7.0 Hz, 2 H), 2.00−1.50 (m, 8 H), 0.88−0.74 (m, 2 H), 0.23 (s, 6 H). MS (FD) $m/z$: 453 $[M]^+$.

**11.** To a solution of **9** (0.44 g, 0.29 mmol) in dry triethylamine (30 mL) and dry THF (30 mL) were added **10** (0.79 g, 1.73 mmol), CuI (20 mg), and $(Ph_3P)_2PdCl_2$ (40 mg). After stirring overnight at room temperature, the mixture was poured in $CH_2Cl_2$ and water. The organic phase was extracted with water and brine and dried over $MgSO_4$. Purification was performed by repeated column chromatography over silica gel using $CH_2Cl_2$/$Et_2O$ (100:1; $R_f$ = 0.25) and $Et_2O$/PE (1:1; $R_f$ = 0.12) as eluents to give **4** (0.40 g, 48%) as a yellow solid. $^1$H NMR ($CD_2Cl_2$): $\delta$ = 7.50 (d, 8.2 Hz, 4 H), 7.31 (s, 4 H), 7.30−7.10 (m, 16 H), 7.06 (s, 4 H), 7.02 (s, 4 H), 5.41 (t, $J$ = 2.8 Hz, 4 H), 5.01 (s, 4 H), 4.42 (t, $J$ = 5.9 Hz, 4 H), 3.99 (t, $J$ = 6.4 Hz, 8 H), 3.97 (t, $J$ = 6.6 Hz, 8 H), 3.90−3.77 (m, 4 H), 3.65−3.52 (m, 4 H), 2.75 (t, $J$ = 7.5 Hz, 4 H), 2.42 (t, $J$ = 7.0 Hz, 8 H), 2.30 (s, 6 H), 2.16 (quin, $J$ = 6.8 Hz, 4 H), 2.10−1.50 (m, 48 H), 1.08 (t, $J$ = 7.4 Hz, 12 H), 1.06 (t, $J$ = 7.4 Hz, 12 H), 0.89−0.79 (m, 8 H), 0.25 (s, 24 H); MS (MALDI-TOF) $m/z$: 2852 $[M + Na]^+$.

**12.** $Bu_4NF$ (1 M in THF, 3 mL) was added to a solution of **11** (0.37 g, 0.13 mmol) in THF (15 mL). After 3 h of stirring at room temperature the mixture was poured into $Et_2O$ and water, and the organic phase was separated and extracted with water and brine and dried over $MgSO_4$. The solvent was evaporated, and the remaining residue was purified by repeated column chromatography over silica gel using $Et_2O$/PE (1:1; $R_f$ = 0.28) as the eluent to give **12** (0.23 g, 76%) as a yellow solid. $^1$H NMR ($CD_2Cl_2$): $\delta$ = 7.50 (d, $J$ = 8.1 Hz, 4 H), 7.35−7.12 (m, 20 H), 7.05 (s, 4 H), 7.01 (s, 4 H), 5.40 (t, $J$ = 3.1 Hz, 4 H), 5.00 (s, 4 H), 4.41 (t, $J$ = 6.1 Hz, 4 H), 3.98 (t, $J$ = 6.5 Hz, 8 H), 3.97 (t, $J$ = 6.3 Hz, 8 H), 3.90−3.78 (m, 4 H), 3.65−3.53 (m, 4 H), 3.15 (s, 4 H), 2.75 (t, $J$ = 7.5 Hz, 4 H), 2.31 (s, 6 H), 2.25−2.10 (m, 4 H), 2.05−1.50 (m, 40 H), 1.07 (t, $J$ = 7.3 Hz, 12 H), 1.06 (t, $J$ = 7.4 Hz, 12 H). MS (MALDI-TOF) $m/z$: 2351 $[M + Na]^+$.

**13.** A solution of **12** (187 mg, 0.08 mmol) in dry pyridine (20 mL) was added to a suspension of CuCl (1.17 g, 118 mmol) and $CuCl_2$ (235 mg, 17 mmol) in pyridine (170 mL) over 96 h at room temperature. After completion of the addition, the mixture was allowed to stir for an additional day and then was poured into $CH_2Cl_2$ and water. The organic phase was extracted with 25% $NH_3$ solution, water, 10% acetic acid, water, 10% aqueous sodium hydroxide, and brine and dried over $MgSO_4$. After evaporation of the solvent to a small amount (about 15 mL), the product was precipitated by the addition of methanol and collected by filtration. Purification was performed by column chromatography over silica gel using $CH_2Cl_2$ as the eluent ($R_f$ = 0.30). **13** (151 mg, 81%) was obtained as a slightly yellow solid. $^1$H NMR ($CD_2Cl_2$): $\delta$ = 7.62 (d, $J$ = 8.2 Hz, 4 H), 7.43 (d, $J$ = 8.2 Hz, 4 H), 7.36−7.33 (m, 4 H), 7.30 (s, 4 H), 7.27−7.24 (m, 4 H), 7.21−7.16 (m, 4 H), 7.09 (s, 4 H), 7.06 (s, 4 H), 5.44 (t, $J$ = 3.1 Hz, 4 H), 5.08 (s, 4 H), 4.36 (t, $J$ = 5.6 Hz, 4 H), 4.03 (t, $J$ = 6.5 Hz, 8 H), 4.01 (t, $J$ = 6.6 Hz, 8 H), 3.94−3.80 (m, 4 H), 3.68−3.57 (m, 4 H), 2.75 (t, $J$ = 7.6 Hz, 4 H), 2.33 (s, 6 H), 2.23−2.08 (m, 4 H), 2.08−1.50 (m, 40 H), 1.09 (t, $J$ = 7.4 Hz, 12 H), 1.07 (t, $J$ = 7.4 Hz, 12 H). MS (MALDI-TOF) $m/z$: 2348 $[M + Na]^+$.

**14.** To a solution of **13** (122 mg, 0.05 mmol) in $CHCl_3$ (70 mL) and methanol (5 mL) was added *p*-toluenesulfonic acid (5 mg). The mixture was stirred for 3 days under light exclusion. After evaporation of the solvent to a small volume, the residue was dissolved in THF, and the product was precipitated by the addition of methanol. After filtration and vacuum drying in the dark, **14** was obtained as a slightly yellow solid (100 mg, quantitative) and

used as received. $^1$H NMR (THF *d*-8): $\delta$ = 7.64 (d, $J$ = 8.2 Hz, 4 H), 7.46 (d, $J$ = 8.5 Hz, 4 H), 7.28 (s, 4 H), 7.20−7.16 (m, 4 H), 7.14 (s, 4 H), 7.10 (s, 4 H), 6.96−6.93 (m, 4 H), 6.92−6.88 (m, 4 H), 5.11 (s, 4 H), 4.38 (t, $J$ = 5.7 Hz, 4 H), 4.05 (t, $J$ = 6.3 Hz, 8 H), 4.02 (t, $J$ = 6.3 Hz, 8 H), 2.82−2.68 (m, 4 H), 2.30 (s, 6 H), 2.23−2.10 (m, 4 H), 1.92−1.76 (m, 16 H), 1.10 (t, $J$ = 7.6 Hz, 12 H), 1.06 (t, $J$ = 7.4 Hz, 12 H). MS (FD) *m*/*z*: 1988 $[M]^+$.

**16a.** $K_2CO_3$ (2.00 g, 14.5 mmol) was added to a solution of **14** (92 mg, 0.05 mmol) and 3,4,5-tris(dodecyloxy)benzyl chloride (200 mg, 0.30 mmol) in dry DMF (50 mL), and the mixture was stirred at 60 °C for 3 days in the dark. The mixture was poured into $CH_2Cl_2$ and water, and the organic phase was separated, washed with water and brine, and dried over $MgSO_4$. Purification by repeated column chromatography over silica gel using $CH_2Cl_2$/PE (2:1) as the eluent ($R_f$ = 0.50) gave **16a** as a slightly yellow solid (120 mg, 59%). Mp: 148−149 °C. $^1$H NMR ($CD_2Cl_2$): $\delta$ = 7.62 (d, $J$ = 8.2 Hz, 4 H), 7.43 (d, $J$ = 7.9 Hz, 4 H), 7.39−7.28 (m, 8 H), 7.22−7.08 (m, 8 H), 7.08 (s, 4 H), 7.05 (s, 4 H), 6.63 (s, 8 H), 5.07 (s, 4 H), 4.98 (s, 8 H), 4.36 (t, $J$ = 5.4 Hz, 4 H), 4.09−3.88 (m, 40 H), 2.74 (t, $J$ = 7.6 Hz, 4 H), 2.32 (s, 6 H), 2.24−2.08 (m, 4 H), 1.94−1.65 (m, 40 H), 1.52−1.16 (m, 216 H), 1.14−1.00 (m, 24 H), 0.94−0.81 (m, 36 H); MS (MALDI-TOF) *m*/*z*: 4668 $[M + Ag]^+$.

**16b.** $K_2CO_3$ (2.00 g, 14.5 mmol) was added to a solution of **14** (100 mg, 0.05 mmol) and 3,4,5-tris(hexadecyloxy)benzyl chloride (255 mg, 0.30 mmol) in dry DMF (50 mL), and the mixture was stirred at 60 °C for 3 days in the dark. The mixture was poured into $CH_2Cl_2$ and water, and the organic phase was separated, washed with water and brine, and dried over $MgSO_4$. Purification by repeated column chromatography over silica gel using $CH_2Cl_2$/PE (3:1) as the eluent ($R_f$ = 0.90) gave **16b** as a slightly yellow solid (188 mg, 72%). Mp: 114−116 °C. $^1$H NMR ($CD_2Cl_2$): $\delta$ = 7.62 (d, $J$ = 8.2 Hz, 4 H), 7.43 (d, $J$ = 7.9 Hz, 4 H), 7.39−7.28 (m, 8 H), 7.22−7.08 (m, 8 H), 7.08 (s, 4 H), 7.05 (s, 4 H), 6.63 (s, 8 H), 5.07 (s, 4 H), 4.98 (s, 8 H), 4.36 (t, $J$ = 5.4 Hz, 4 H), 4.09−3.88 (m, 40 H), 2.74 (t, $J$ = 7.6 Hz, 4 H), 2.32 (s, 6 H), 2.24−2.08 (m, 4 H), 1.94−1.65 (m, 40 H), 1.52−1.16 (m, 312 H), 1.14−1.00 (m, 24 H), 0.94−0.81 (m, 36 H). MS (MALDI-TOF) *m*/*z*: 5341 $[M + Ag]^+$.

**Acknowledgment.** Financial support by the Deutsche Forschungsgemeinschaft and the Multifunctional Materials and Devices Center (BMBF 03N 6500) is gratefully acknowledged. The authors thank the Federal Science Policy through IUAP-V-03, the Institute for the Promotion of Innovation by Science and Technology in Flanders (IWT), and the Fund for Scientific Research-Flanders (FWO). The Katholieke Universiteit Leuven is thanked for financial support via an IDO interdisciplinary research program. S.D.F. is a postdoctoral fellow of FWO. Research in Mons is supported by the European Commission and Région Wallonne (Phasing Out − Hainaut program) and FNRS. M.S. is grateful to FRIA for a doctoral fellowship.

**Supporting Information Available:** $^{13}$C NMR spectra for all new compounds as well as additional analytical data for the macrocycles **16a** and **16b** (PDF). This material is available free of charge via the Internet at http://pubs.acs.org.

CM051386L